

Stephen D. Jascourt¹ UCAR/COMET
Silver Spring, MD¹

1. INTRODUCTION

Two different versions of the Weather Research and Forecasting (WRF) model (WRF, 2007) dynamic cores, used also with various different physics packages, are run operationally by the National Centers for Environmental Prediction (NCEP) in support of National Weather Service (NWS) forecast operations. One of these, the Nonhydrostatic Mesoscale Model (NMM) (Janjic, et. al. 2001, Janjic, 2004, Rogers, et. al., 2005), replaced the Eta (Black, et. al., 1993 and change log in NCEP, 2007) as the 12-km grid spacing, 60-layer model run in the North American Mesoscale (NAM) slot which NWS forecasters receive in AWIPS and heavily utilize in their daily forecasts.

Forecasters have been noticing that the nonhydrostatic NAM-WRF produces considerable high-amplitude gravity wave activity during episodes of even moderate flow over even moderately-sized terrain features, explicitly predicting wave-related phenomena which the hydrostatic Eta model suggested but did not fully explicitly represent. For example, see Fig. 1. This would seem to be a significant advance in numerical weather prediction, and these waves typically are predicted under appropriate wind and stability conditions and represent real features, as will be shown in some examples later. However, forecasters have also noticed a deep downward vertical velocity signature on the upwind side of hills and upward vertical velocity signature on the downwind side, and these tilt far over their respective sides rather than being confined to near the ridge crest. This signature is robust and ubiquitous across many synoptic situations and geographic locations and appears to indicate deep descent where observed upslope precipitation occurs. While tilt of descent over the upwind side of bell-shaped mountains is part of classical wave solutions, the NMM solutions show deep descent with smaller vertical wave number than classical solutions and without the low-level upslope ascent of the classical solutions, in some cases causing forecasts of far too little upslope precipitation.

The WRF ARW core does not exhibit these peculiar phase positions of the waves, instead producing waves with narrower wavelength which appear to correspond better to limited pertinent observations. The actual topography giving rise to the observed phenomena has much finer structure than model

terrain, thus it is not known whether the NMM solution might be more correct for the terrain it uses despite the better apparent correspondence between ARW and observations.

Differences between the wave structures in NMM and ARW solutions may cause differences in wave momentum flux and mean-flow acceleration. The resulting mountain wave drag and its influence on synoptic flow evolution was not examined.

The ARW and NMM employ much different numerical schemes. ARW uses a high-order Runge Kutta time differencing in a traditional approach while lower-order NMM calculates the nonhydrostatic terms as an add-on to the hydrostatic terms in an innovative approach using discretization involving careful treatment of the omega-alpha term.

The comparison of NMM and ARW dynamic core solutions presented here comes from the High-Resolution Window (hiresw) runs conducted by NCEP (NCEP, 2007b – see the September 2004 and June 2005 entries). These runs, NMM at 5.1-km grid spacing and ARW at 5.8-km grid spacing, both do not employ a convective parameterization. Both use initial and boundary conditions interpolated from the operational NAM. However, the land surface conditions and terrain are not identical, though the terrain is fundamentally similar as will be apparent in the many plots shown here. They do not use the most recent versions of the WRF code. Nonetheless, the characteristics evident in the operational NAM-WRF also appear in the hiresw NMM runs despite the resolution and model code version differences.

The waves over hills discussed here are for cases where the flow is not blocked by the terrain, so Froude number is not discussed. The wavelengths are somewhat between the hydrostatic and nonhydrostatic wave regimes and are clearly far short of the rotational wave regime. Vertical bending of waves, ducting, and critical layer behavior are, of course, inherently nonhydrostatic processes. Detailed review of mountain wave dynamics is given in some physics-oriented dynamics textbooks such as Gill (1982), chapter 8. While plots presented in this article show omega (dp/dt) rather than w (dz/dt) due to the latter being unavailable for some of the model runs shown, extremely close correspondence between omega and w were found when both were available. This good match between omega and w is to be expected for a standing wave since the local pressure tendency will be small.

Corresponding author address: Stephen D. Jascourt,
NWS Meteor. Services Division – W/OS 2, SSMC2
Rm. 13110, 1325 East-West Hwy, Silver Spring MD
20910 Stephen.Jascourt@noaa.gov

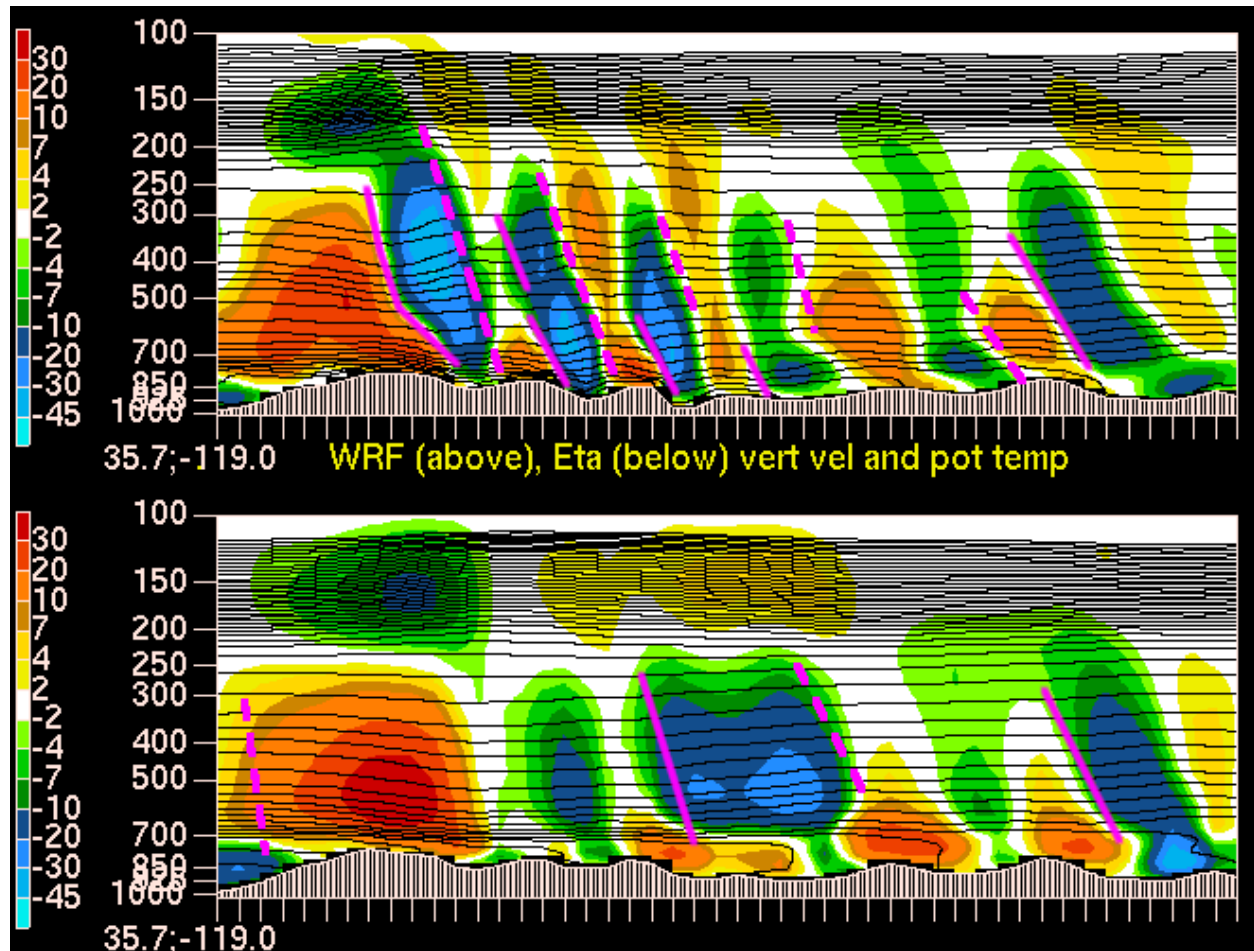


Figure 1. Omega (pressure vertical velocity) for NAM WRF-NMM (above) and NAM-Eta (below) using color scale shown, with ascent in blues and descent in oranges for strong westerly flow from left to right across the Sierra Nevada mountains in California at the left, extending eastward across southern Nevada toward the right. Isentropes are drawn at 2K interval in black. Solid magenta lines are axes of maximum potential temperature while dashed are minimum potential temperature. Note that the NMM waves have a proper quadrature phase relationship between the vertical motion and temperature perturbations and show much more sharply defined structure than the waves in the Eta model.

2. WAVES GENERATED BY BLACK HILLS, SD

A typical example of waves seen in many places under many conditions is illustrated by the case of northeast flow over the Black Hills of western South Dakota on December 20, 2006 as in Figure 2 and Figure 3. In this and all later plots, blues indicate descent and yellow indicate ascent, while wind barbs are all for horizontal winds with northerly winds pointing downward and are not plotted at every output grid point. Notice how far back across the upwind side the area of descent is in both the NAM and hiresw NMM 6-hour forecasts. They did have upward motion at the lowest levels, but weaker than the smallest amount shaded in the color scale. In contrast, even

the hydrostatic RUC model shows more upward motion on the upwind side and the ARW cross section shows that the descent near the surface begins at the ridge crest and tilts only slightly upstream with height, with a much narrower wavelength than in the NMM.

Six hours later, difference fields for temperatures and winds are shown. The thermal differences may be related to differences in radiation and clouds though there may also be contributions from wave fluxes.

In flow over the hills from a different direction, upslope snow of several inches was observed where the model indicated sinking motion, as shown in Figures 5 and 6.

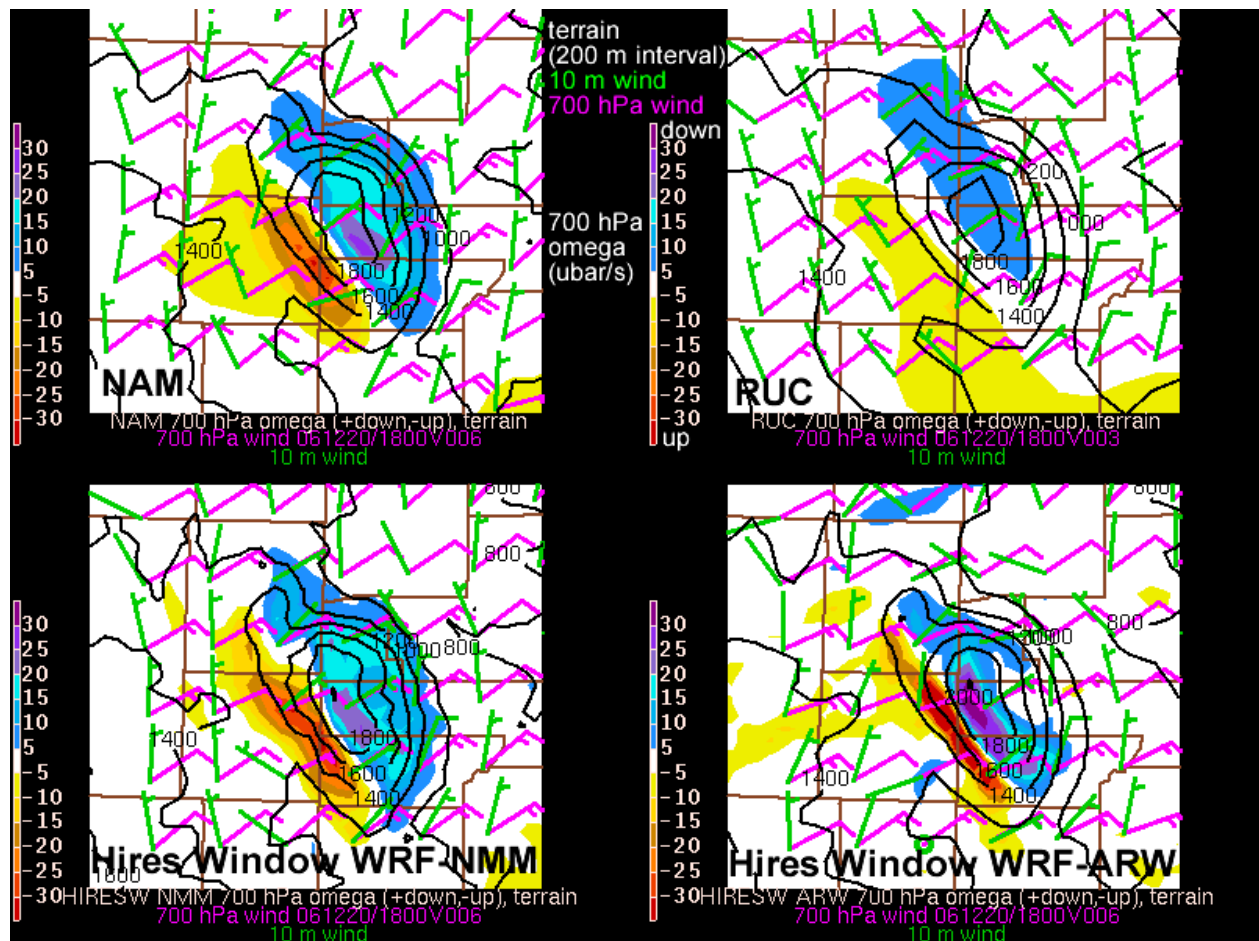


Figure 2. Omega and terrain height over western SD and far eastern WY. Ascent indicated in oranges and descent in blues. Winds at 10-meters above model terrain are in green. Winds at 700 hPa are in magenta. Brown lines indicate county borders.

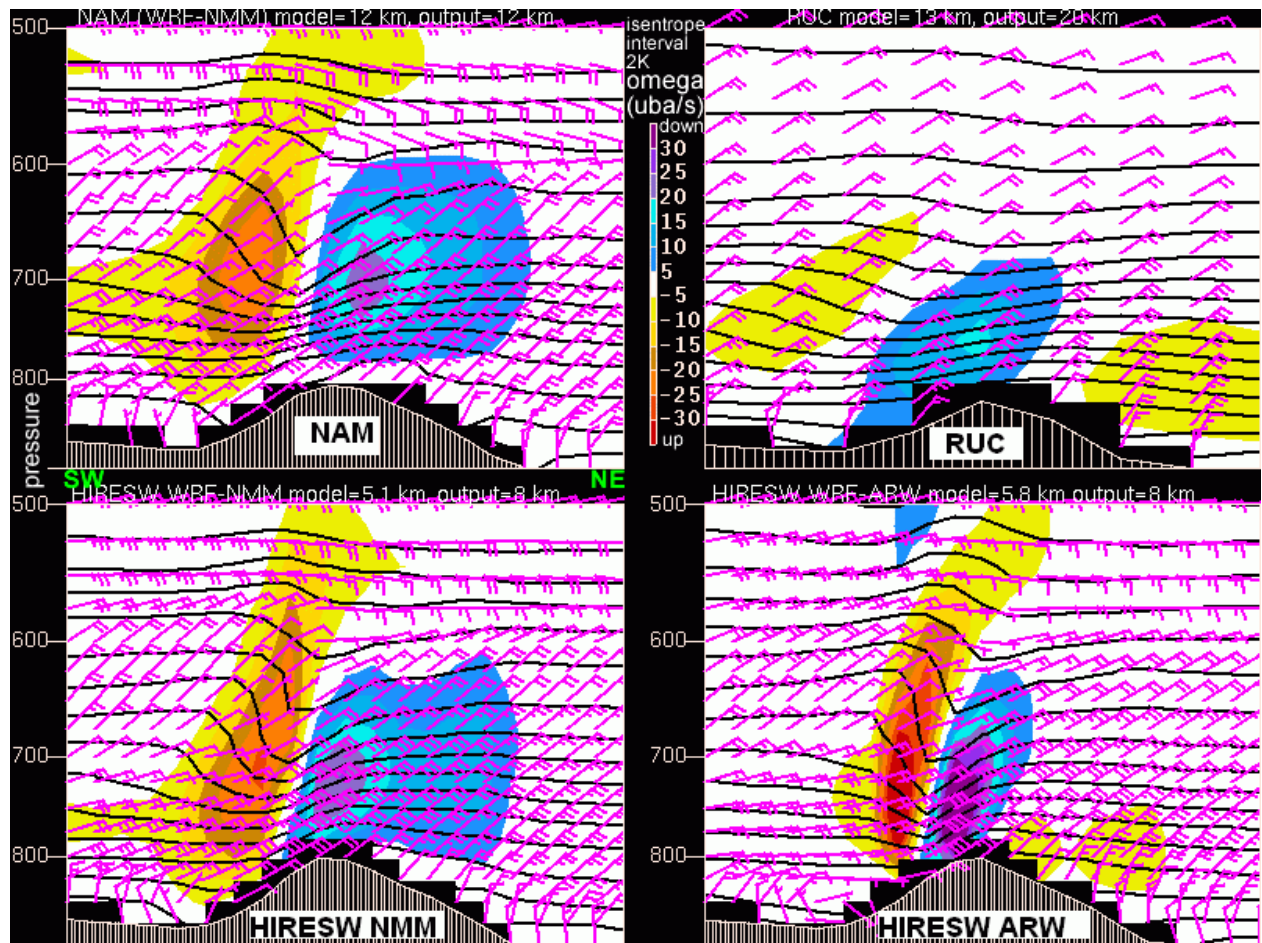


Figure 3. Cross sections through the middle of the Black Hills. Wind bars are horizontal winds with northerly component pointing downward – winds are from the northeast.

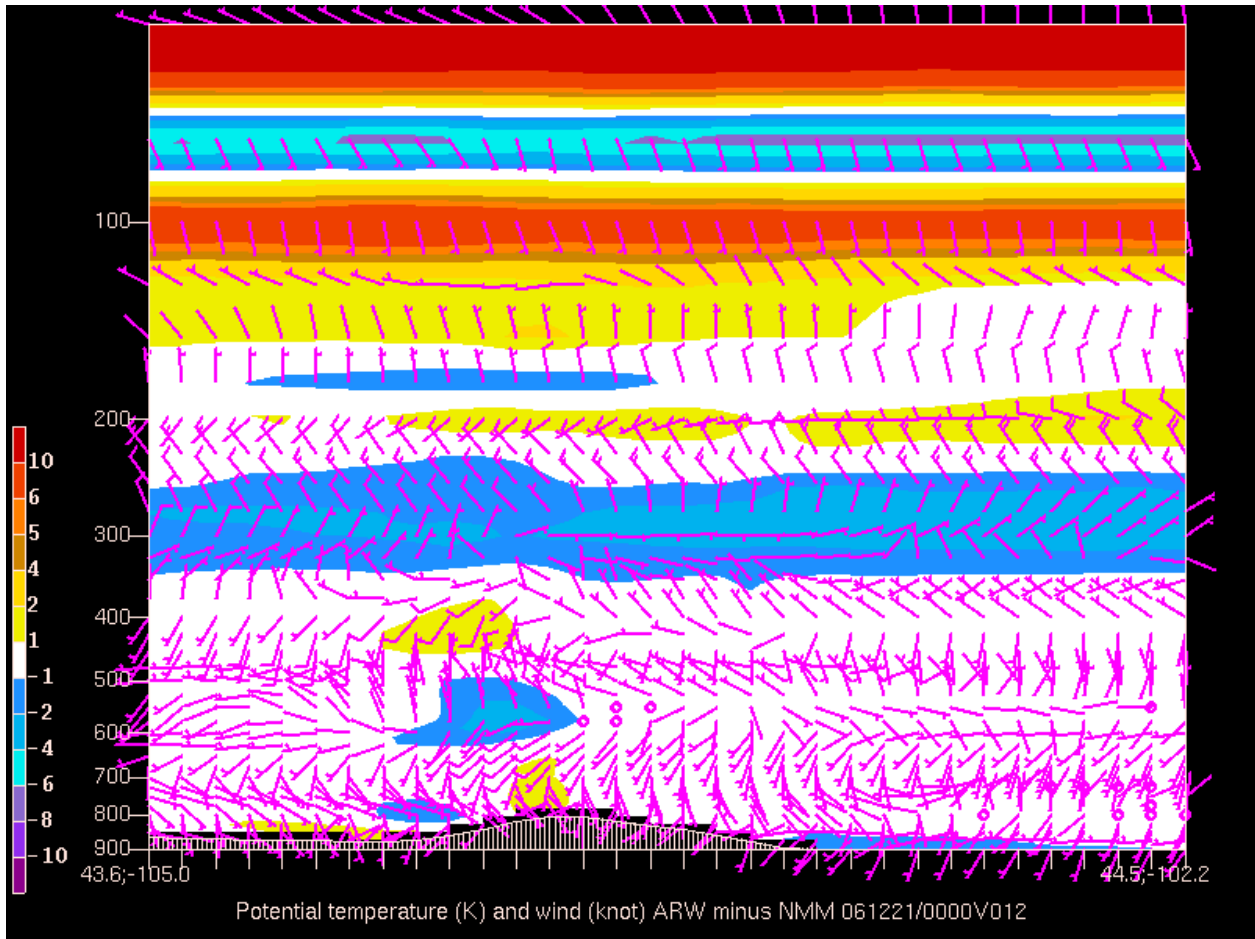


Figure 4. Difference fields between ARW and NMM solutions at 12 hours (6 hours after cross sections in Figure 3).

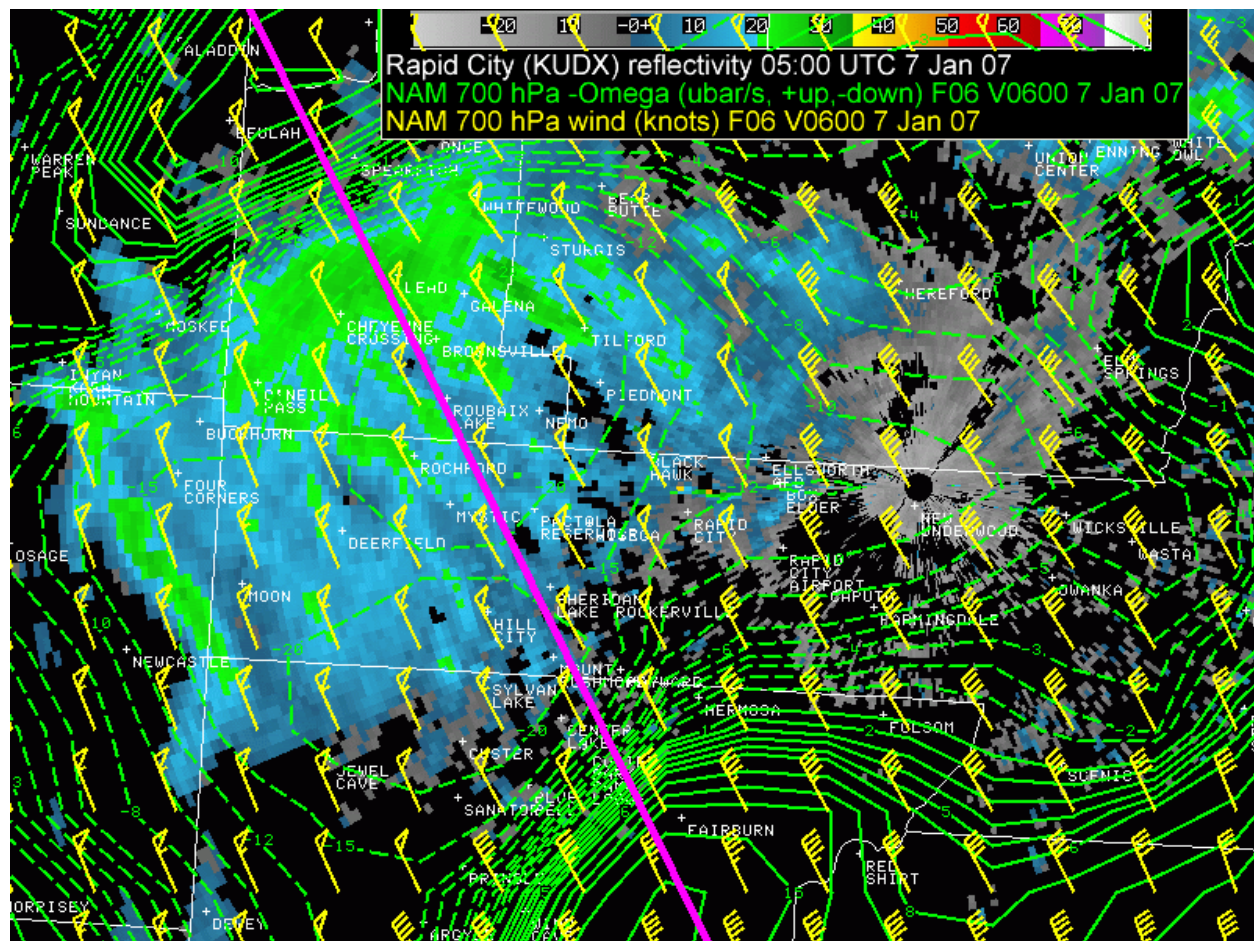


Figure 5. Radar reflectivity (color shades) indicating upslope snow over the Black Hills in a northwesterly flow case. NAM 6-h forecast winds and vertical motion at 700 hPa are overlaid, with solid contours indicating upward motion, dashed contours downward motion. Magenta line is cross section shown in Fig. 6. Adapted from images provided by Kyle Carstens and Matthew Bunkers of the Rapid City, SD NWS Weather Forecast Office.

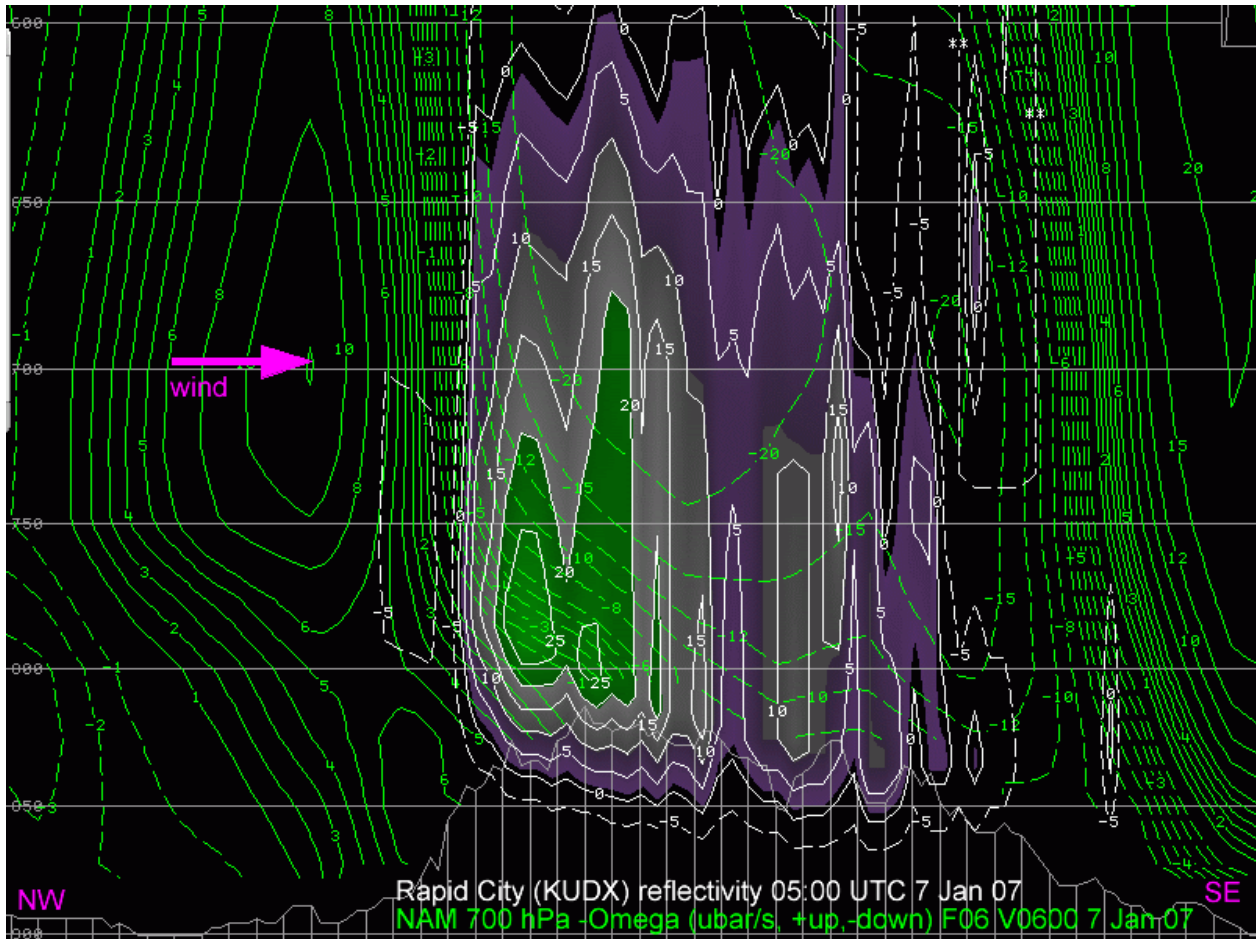


Figure 6. Cross section of same fields and plotting convention as in Figure 5. Vertical white stripes indicate terrain. Precipitation is over the hills on the upwind side while model shows deep descent in that area. Adapted from images provided by Kyle Carstens and Matthew Bunkers of the Rapid City, SD NWS Weather Forecast Office.

3. WAVELENGTH OVER APPALACHIANS

In a case of northwest flow across the mid-Atlantic states, the ARW run shows more waves and higher amplitude. Figures 7 and 8 show horizontal sections at 900 and 800 hPa, with ARW indicating north-south boundary layer rolls over the coastal plain of Virginia and Maryland. In this case, the hiresw NMM does show more waves than the NAM WRF-NMM, suggesting perhaps resolution is a factor affecting wavelength, unlike for the Black Hills case. The cross section from PIT to SBY (Fig. 9) shows shorter wavelength in ARW waves. But the cross section from

HLG to AKQ (Fig. 10), a bit further south, shows the same deep wave pattern in NMM and ARW though with boundary layer differences. The terrain comparison is shown in Fig. 11. A visible satellite image in Fig. 12 reveals observed waves had shorter wavelengths than resolvable by any of these models, raising the question of whether the terrain wavelength in the model is the primary factor affecting the model wavelength. Is the ARW shorter wavelength perhaps incorrect for its terrain despite being more similar to what was observed or is the NMM solution incorrect, or both? Recall, the hiresw NMM has a grid spacing of 5.1 km while ARW is slightly coarser at 5.8 km.

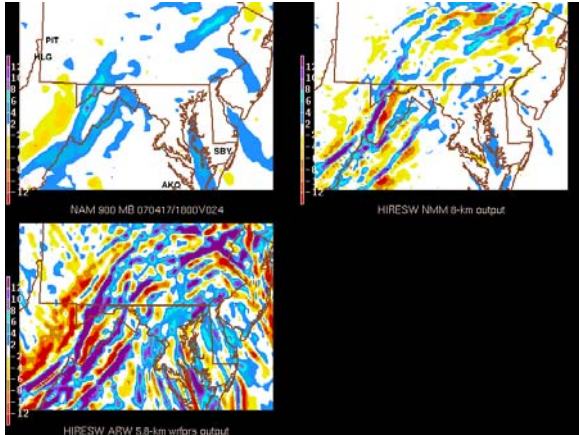


Figure 7. 900 hPa omega for a 24-hour forecast (NAM upper left, NMM upper right, ARW, lower right). Blues indicate descent and yellows indicate ascent.

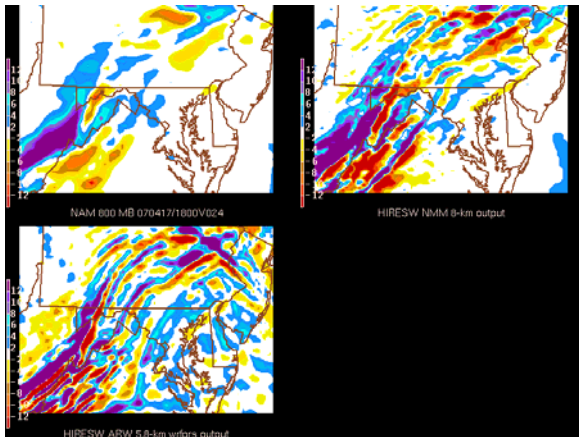


Figure 8. Same as fig. 7 but for 800 hPa

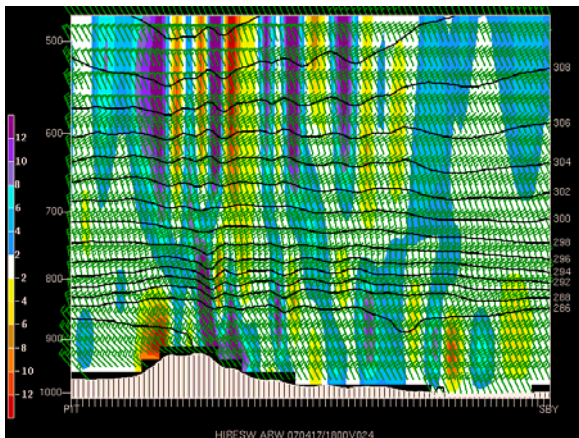


Figure 9a. 24-h forecast omega (as usual, yellow is ascent, blue is descent) along cross section from PIT on the left southeastward toward SBY on the right, for ARW.

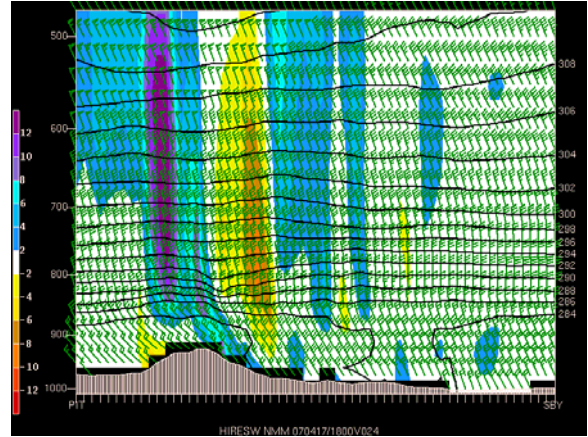


Figure 9b. Same as Fig. 9a but for hires NMM

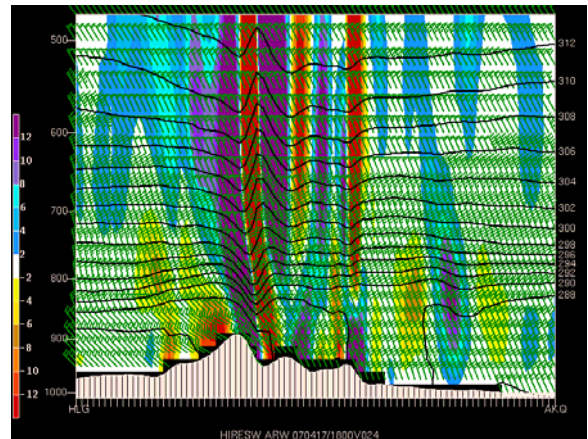


Figure 10a. Same as Figure 9 (ARW) but for cross section from HLG (left) southeastward toward AKQ (right). This section is further south than Fig. 9

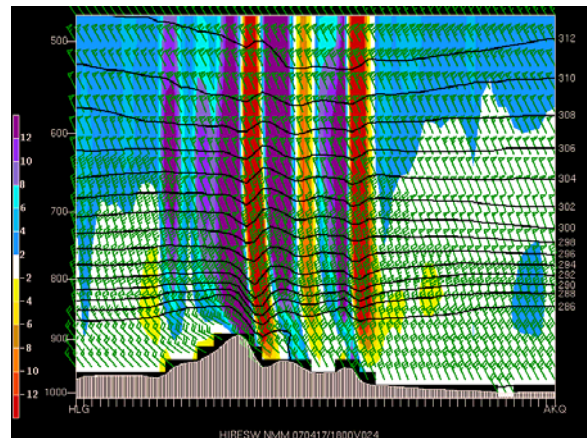


Figure 10b. Same as Figure 10a but for NMM

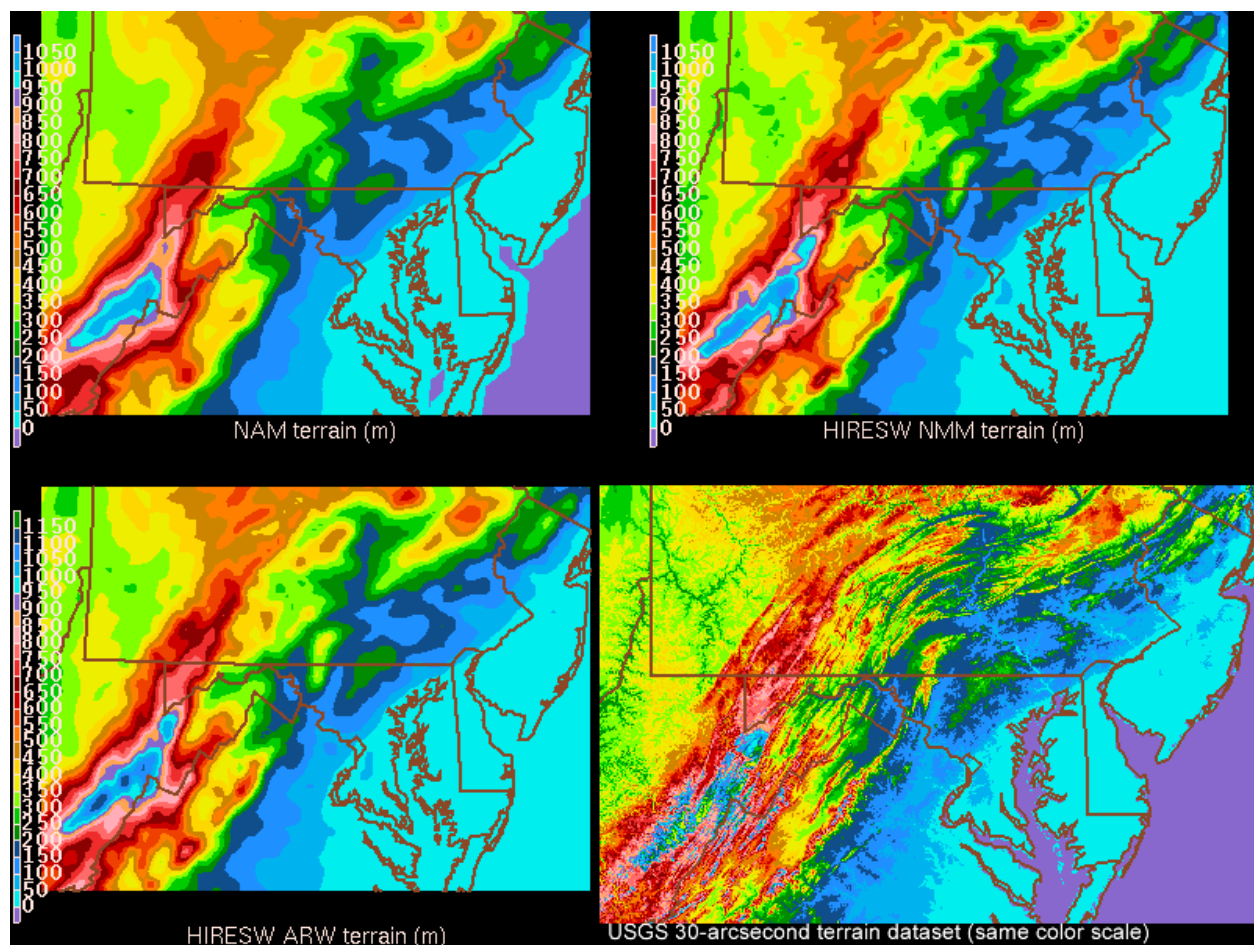


Figure 11. Terrain (m) for the 3 models and the USGS 30-arcsecond dataset.

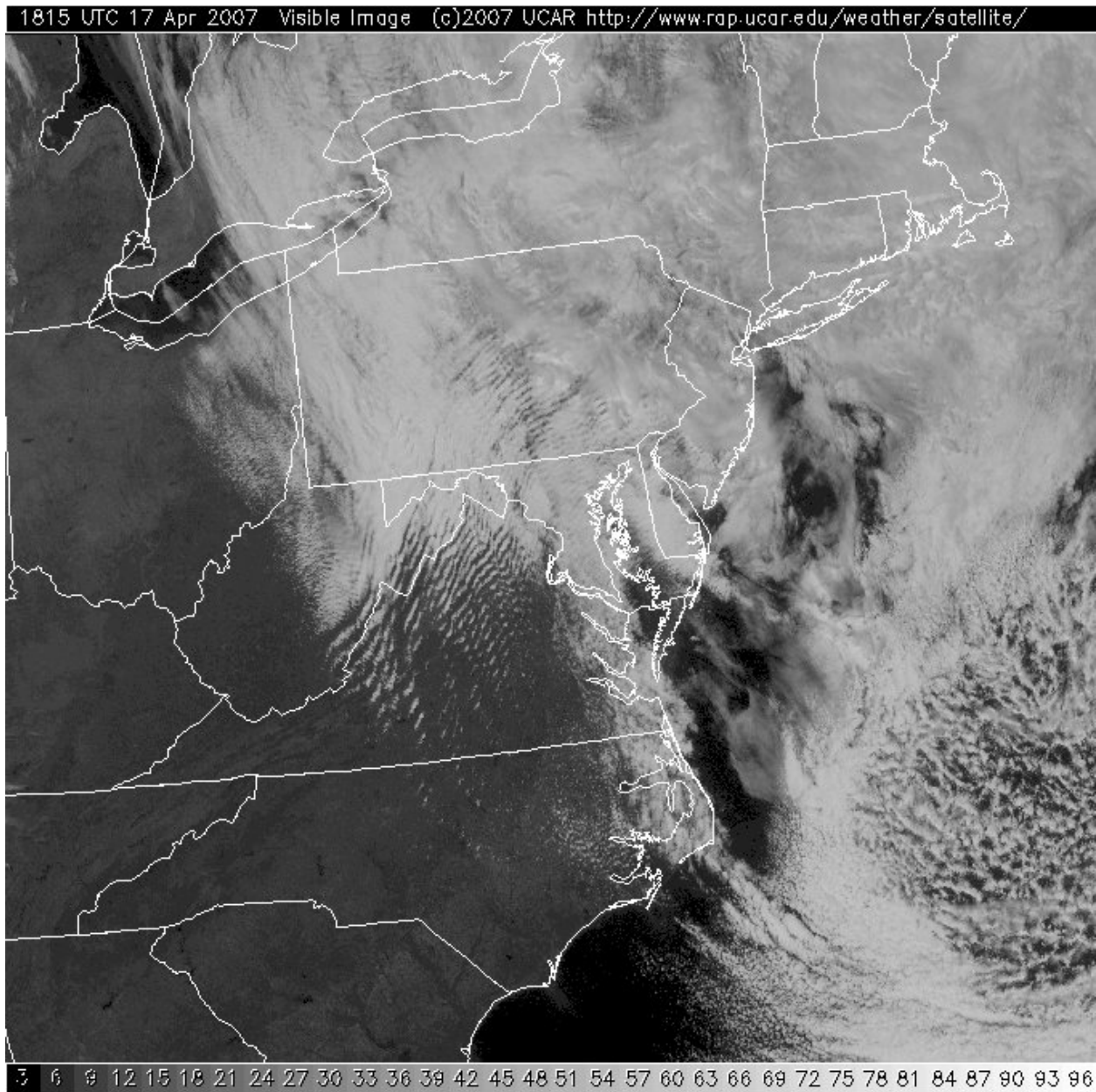


Figure 12. Visible satellite image 15 minutes after the forecast valid time for the plots in Figs. 7-10

4. LAKE BLUFFS, OBSERVED WAVES

Precipitation bands often set up in the same spot during strong northwesterly flow over the western part of Lake Superior. Duluth Weather Forecast Office Science and Operations Officer (SOO) has studied this scenario and found the observed bands to be a result of waves generated by the escarpment north of the lake shore, not lake-effect (D. Miller, personal communication). A typical case is shown in Fig. 13, showing a snow band along the south shore of the west end of the lake, and model 9-hour forecasts of 700 hPa omega for NAM, hiresw NMM, and hiresw ARW. Note that all three models show 700 hPa descent where the snow band usually is present.

However, in the cross sections in Fig. 14, the ARW run shows low-level ascent where the band should be. In the other cross section, again we see shorter wavelength and more complex behavior in ARW, though data to verify it is lacking.

However, the NMM is still useful for forecasters. Not only does it indicate when the waves should be present, but forecasters need to examine boundary layer structure instead of vertical motion at 700 hPa. Fig. 16 shows that waves in the NAM model are above the unstable boundary layer, and areas of clouds and snow at low levels do not correspond to the vertical motion above the boundary layer.

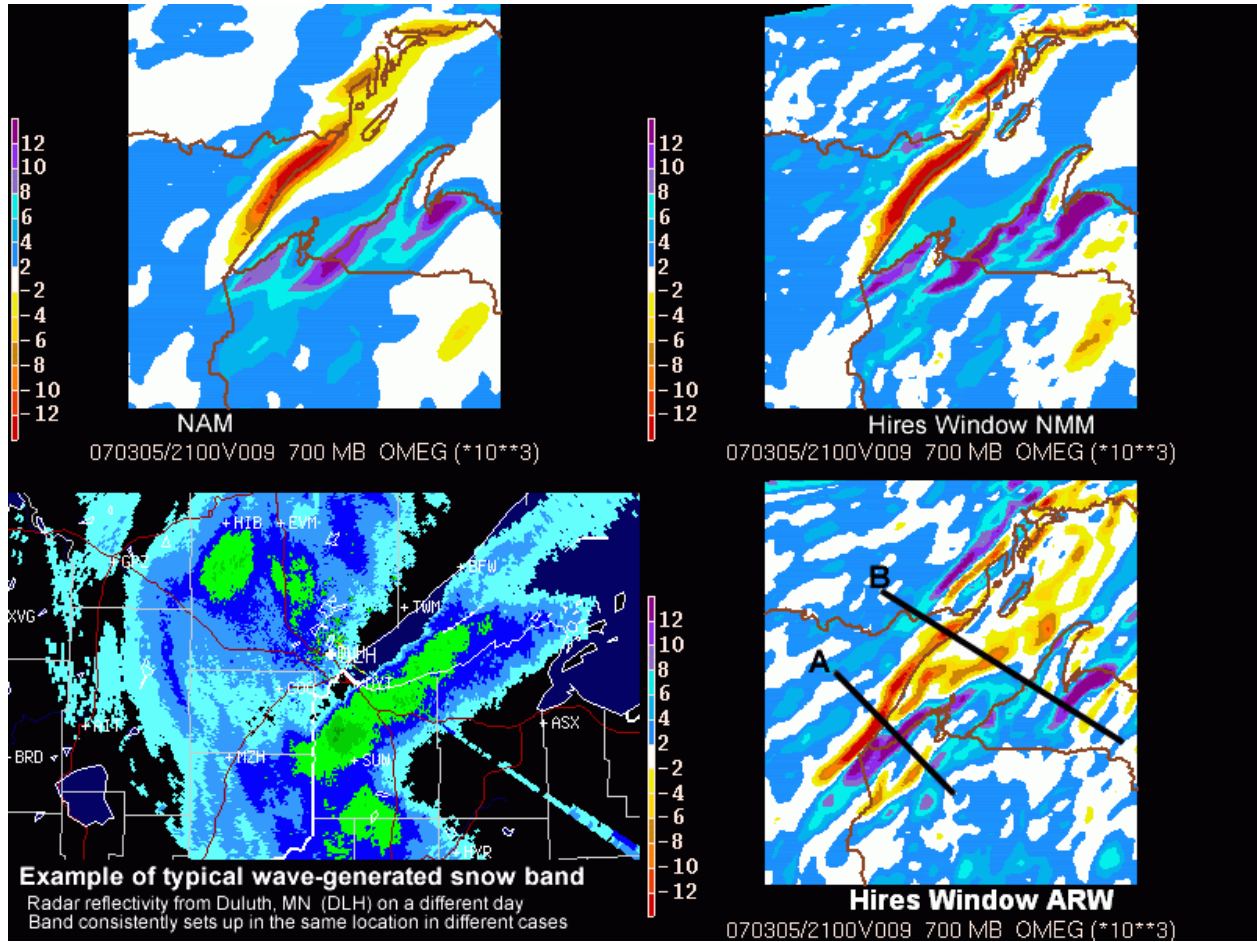


Figure 13. Omega for the three models and a typical corresponding radar plot. Cross section location "A" is used in Fig. 14 and B in Fig. 15. Radar image provided by D. Miller, Duluth, MN NWS forecast office.

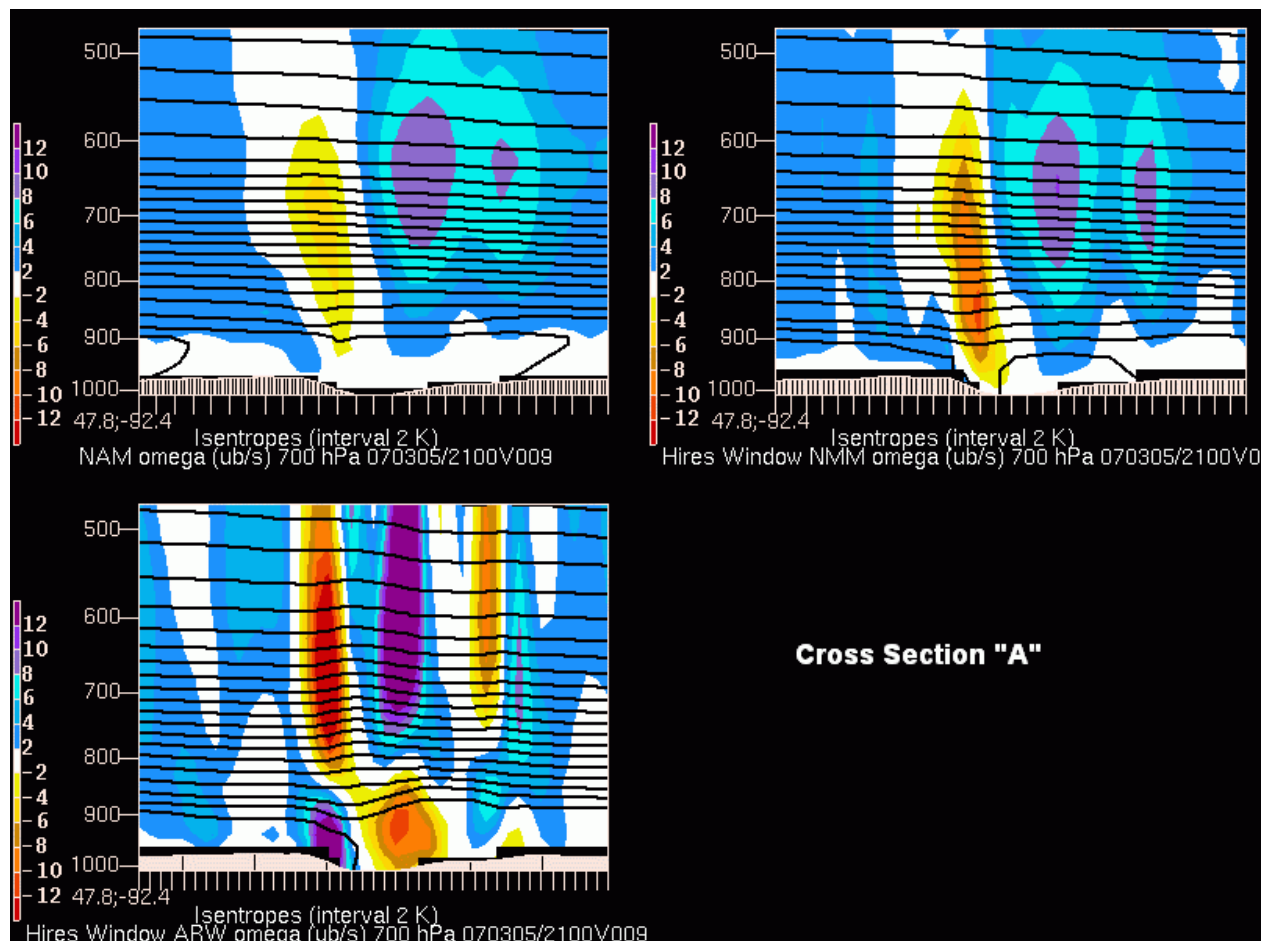


Figure 14. Cross section "A" indicated in Figure 13.

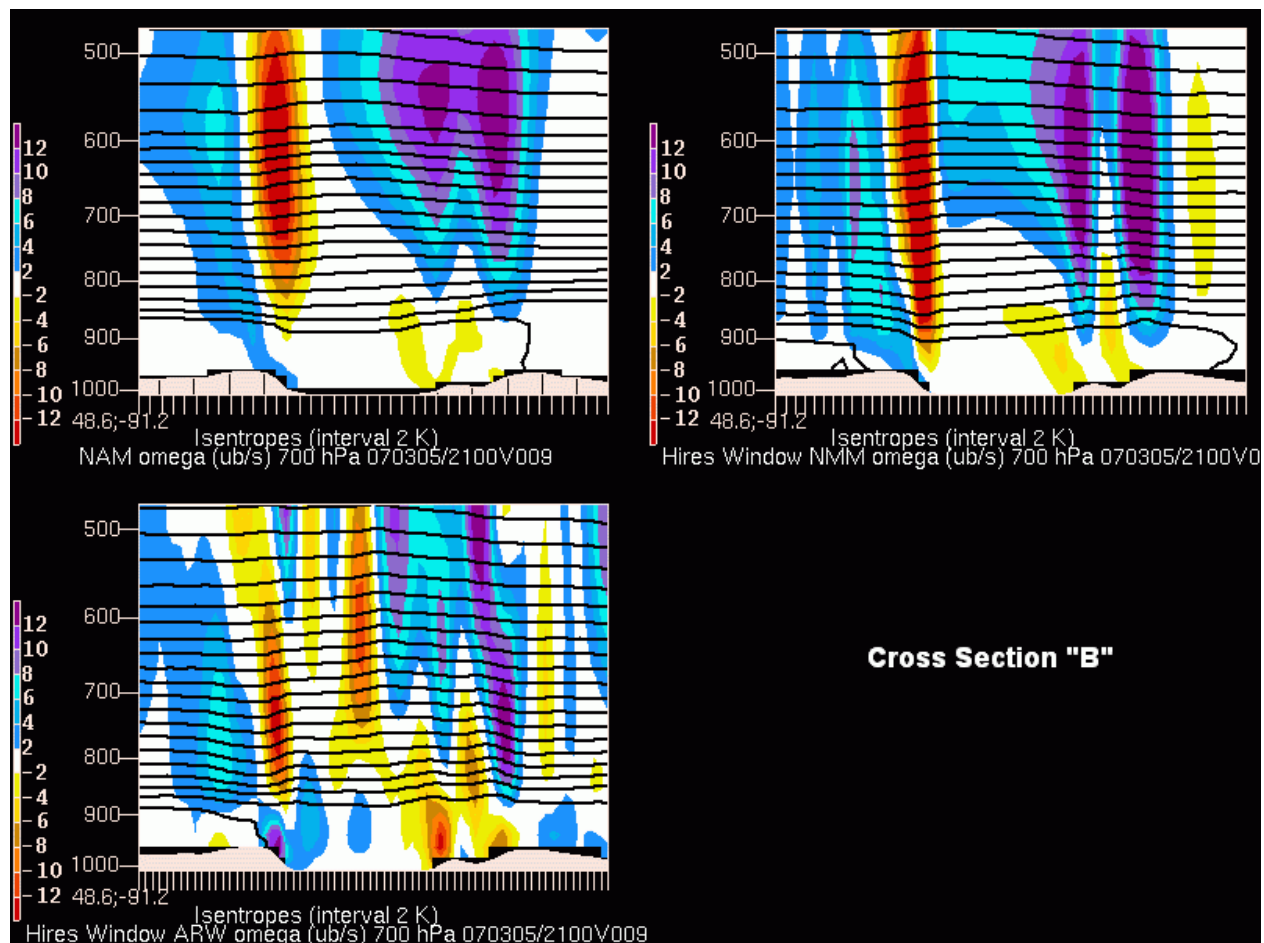


Figure 15. Cross section "B" indicated in Figure 13.

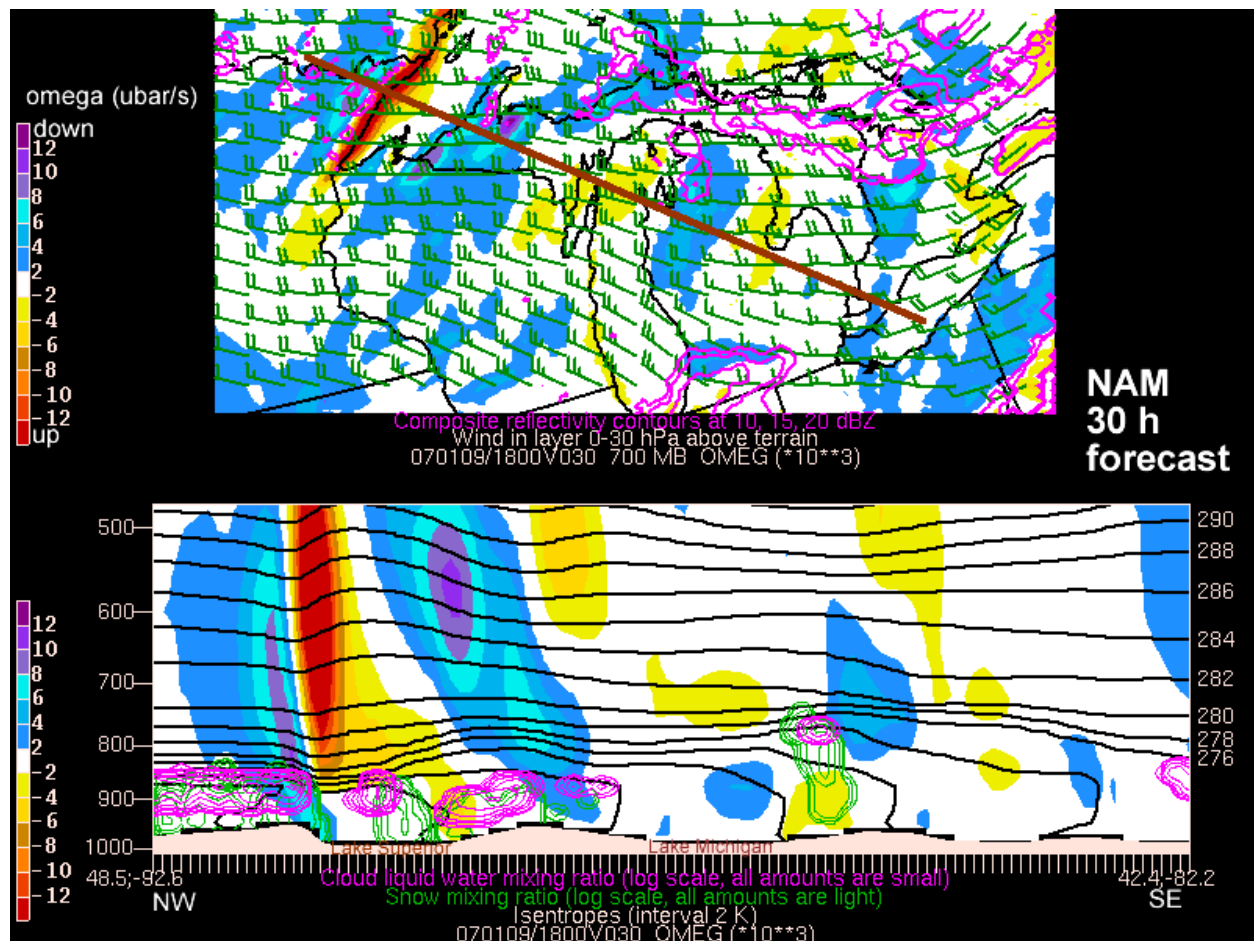


Figure 16. NAM 30-hour forecast 700 hPa omega (top) and cross section along brown line (bottom) with flow from left to right on the cross section. Cloud liquid water mixing ratio is contoured in magenta and snow mixing ratio is in green, indicating clouds and precipitation are not in phase with the waves above the boundary layer inversion.

5. UPSLOPE PRECIPITATION SOMETIMES NOT ADVERSELY AFFECTED IN NMM

The sinking motion on the upwind side of mountains in the NMM occurs above the level at which condensate is forming and falling out, apparently not harming upslope precipitation. For example, the 3-hour precipitation in a winter lake-effect northwest flow case over West Virginia is shown in Figure 17. The 3-hour precipitation patterns are similar in all three models, with most falling on the upwind side of the highest ridge. At 900 hPa (Fig. 18), ARW shows much more or higher-amplitude wave activity, and snow mixing ratio in NAM shows snow falling west of the ridge line. The 750 hPa level (Fig. 19) is above most of the precipitation in the NAM, especially in the region of maximum 3-h accumulation, with widespread descent over the upwind slope in both NMM and NAM, while ARW shows ascent about halfway up the slope and descent near the top. At 650 hPa (Fig. 20), the downward motion with the wave is above all of the precipitation production. Similar

results were seen over the Wasatch range and the coastal mountains in Washington and Oregon. However, in some cases such as over the Black Hills, the NAM-WRF typically predicts only a small fraction of the observed precipitation amounts.

6. HIGH-IMPACT DOWNSLOPE WINDSTORM

The NMM and ARW phase positions agree much better for high-amplitude downslope windstorms. Figure 21 shows the area of descent beginning near the ridge line and has very strong winds along with very stable conditions near the surface where 50 m/s winds were observed. The wind speeds in knots are contoured in white. Mesonet and synoptic stations reported intermittency, with brief periods of strong gustiness and high winds, suggesting a stable layer shielding very high near-surface winds which occasionally mixed down due to turbulence. The NAM 30-hour forecast, and many other NAM forecasts even at longer lead times, depicted this scenario very well. However, the more typical NMM phase

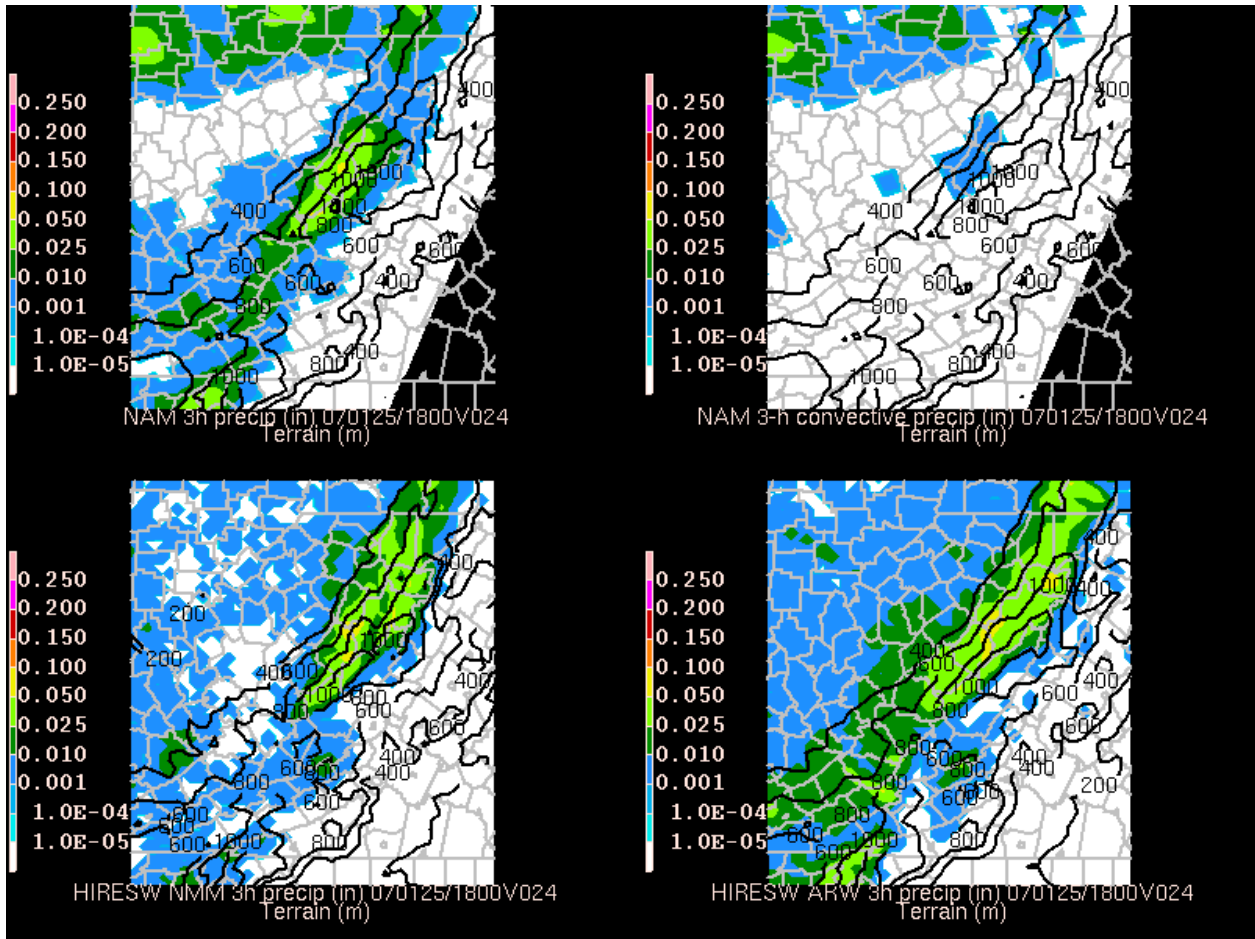


Figure 17. 3-hour precipitation totals and terrain contours. Gray lines are county borders

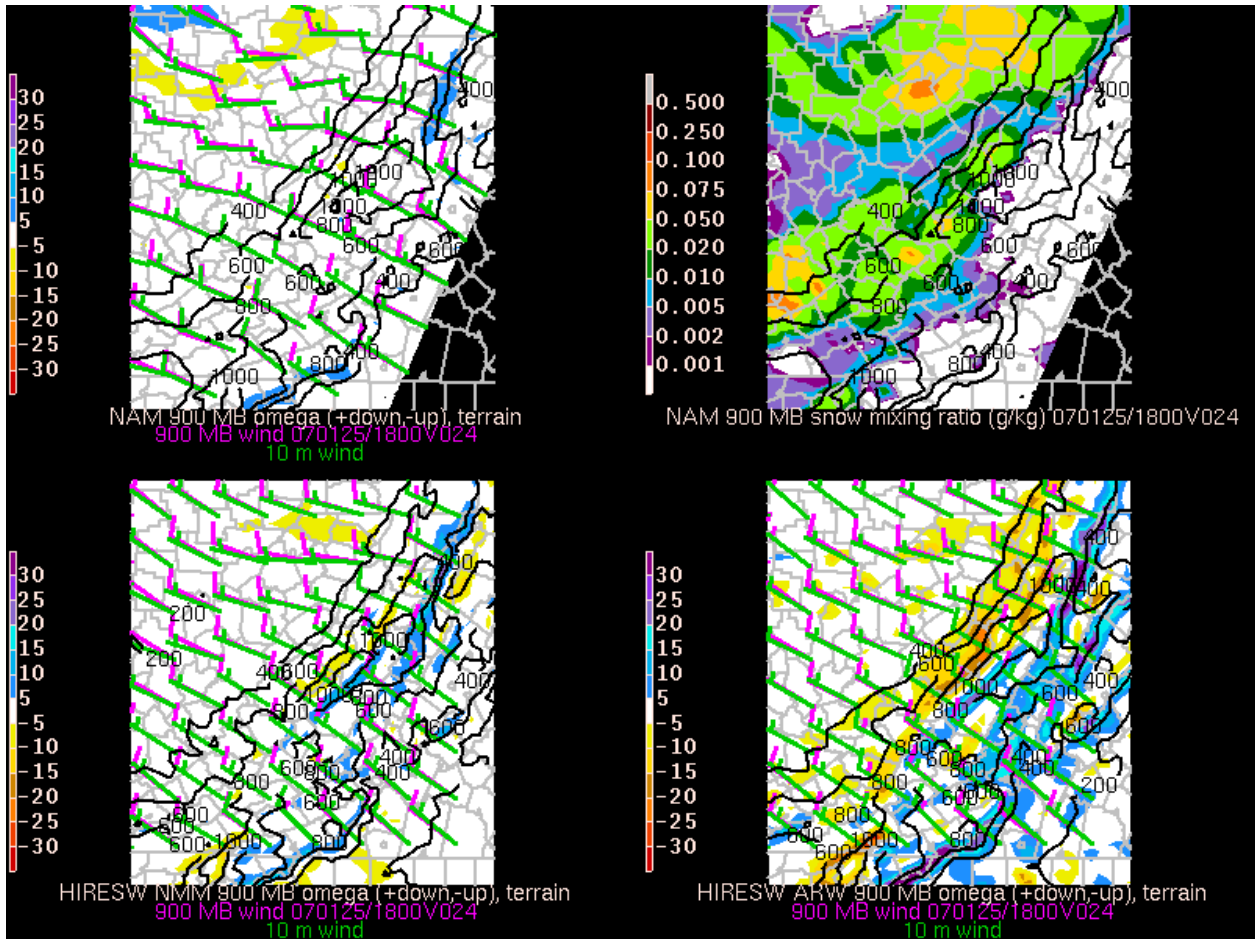


Figure 18. 24-hour forecast 900 hPa omega, winds, and terrain contours. Upper right shows snow mixing ratio for NAM

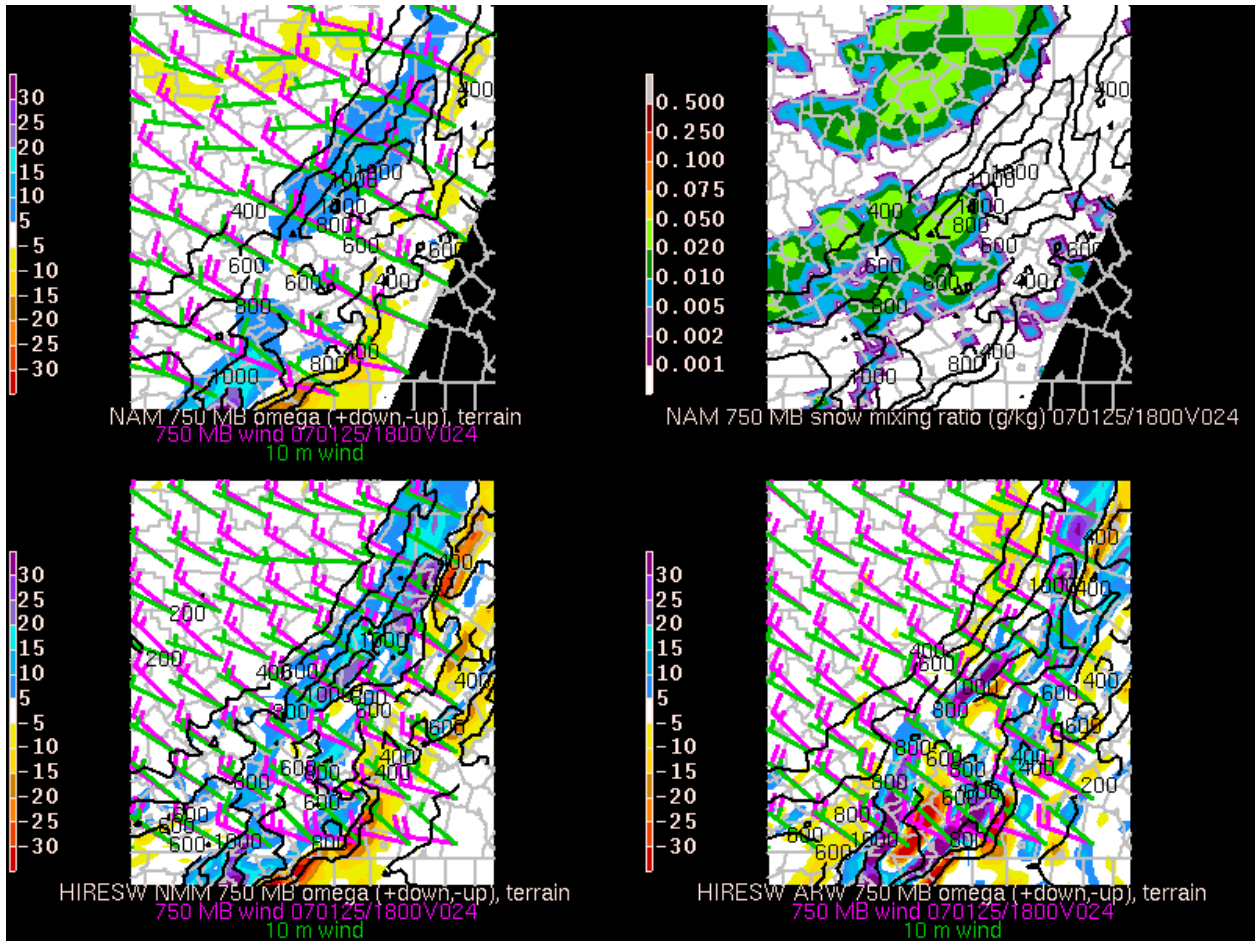


Figure 19. Same as Fig. 18 except at 750 hPa

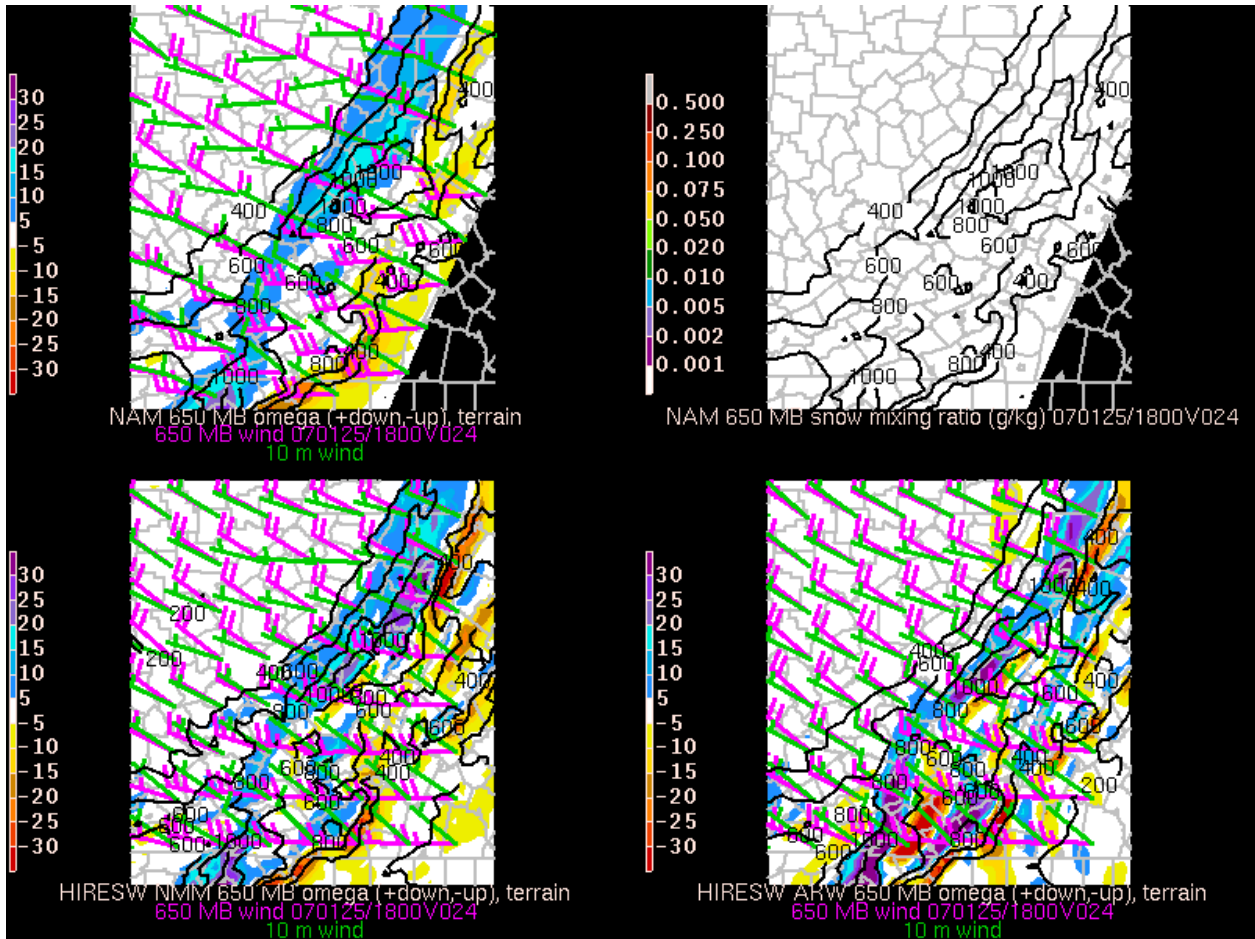


Figure 20. Same as Fig. 18 except at 650 hPa

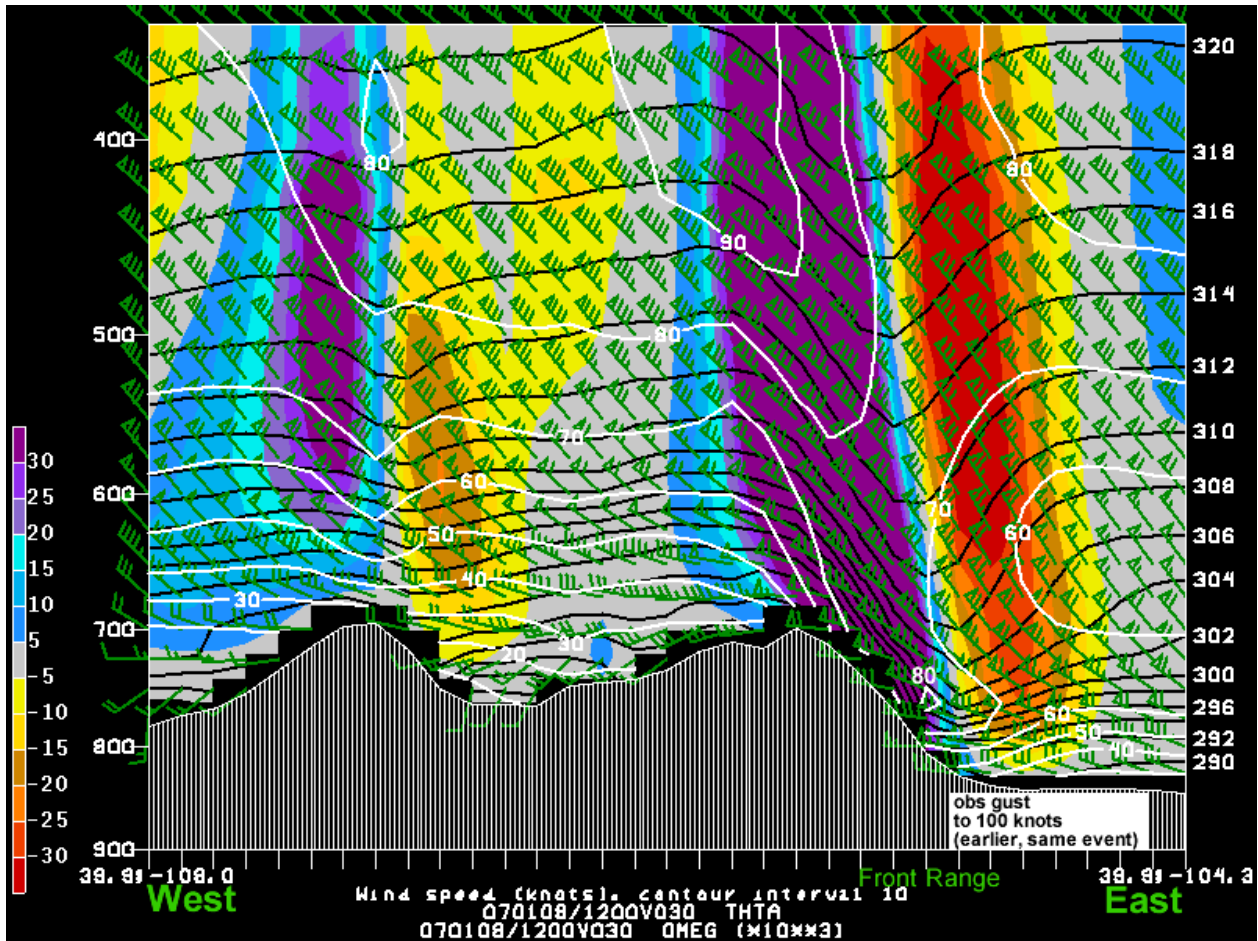


Figure 21. Cross section of NAM 30-hour omega, isentropes (black, labels at right), and wind speed (white, knots). Note the 80 knot winds near the surface along the Front Range. As with all cross sections in this article, wind barbs are horizontal winds, so “vertical” component of the barb is the north-south wind component.

relationship of descent extending far to the upwind side is evident over the mountain at the west end of the cross section.

The hiresw NMM run was similar (Fig. 22). The hiresw ARW run (Fig. 23) had stronger winds reaching the surface across a broad region of the Front Range slope and also over the peak in the western part of the cross section.

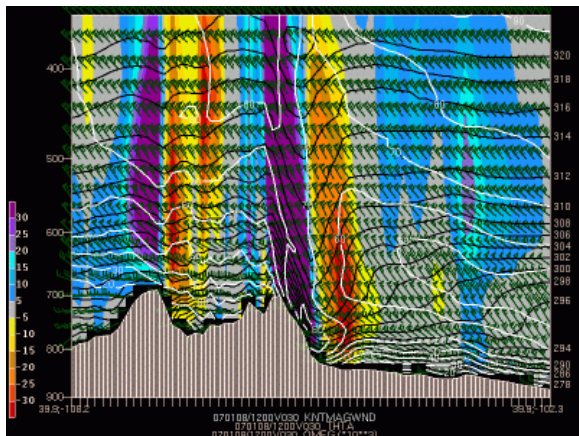


Figure 22. Same as Fig. 21 except for hiresw NMM and the area shown is broader here

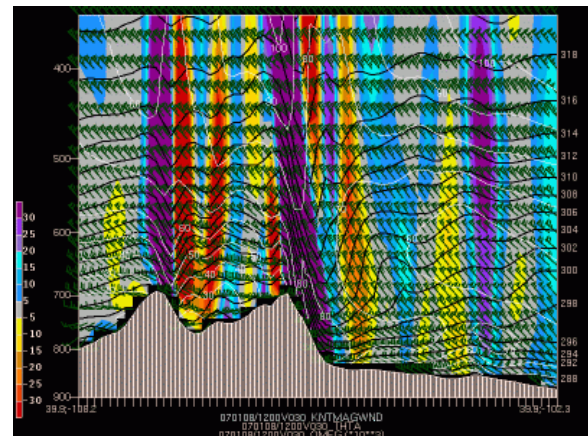


Figure 23. Same as Fig. 22 except for hiresw ARW

7. SUMMARY

In summary, notable differences in gravity wave structure were shown between the ARW and NMM dynamic cores. The NAM, now using the WRF-NMM, provides much better guidance to forecasters about the presence of significant wave activity than its predecessor Eta model, but the phase relationships can be misleading to forecaster interpretation of where precipitation should occur. The discrepancies with observations are troubling and the cause is not known. ARW seems to agree better with observations, but it is not known whether it is better for the correct reasons. The NMM was tested extensively with idealized flow over mountains and matched analytical and other numerical solutions very well (Janjic, personal communication). The similar structure between the 5.1-km hiresw NMM runs and the 12-km NAM runs suggests that the terrain resolution is possibly or often not the only controlling factor.

8. ACKNOWLEDGEMENTS

The author first became aware of this widespread problem when Matt Bunkers, Science and Operations Officer (SOO) at the NWS Rapid City, SD forecast office, pointed out discrepancies between NAM vertical motion and upslope snow events. Also, the author greatly appreciates presentations provided by Dan Miller, SOO at the Duluth, MN forecast office, about Lake Superior snow bands generated by gravity waves.

This paper was prepared by the University Corporation for Atmospheric Research under cooperative agreement award #NA06NWS4670013 from the National Oceanic and Atmospheric Administration (NOAA), U.S. Department of Commerce. The statements, findings, conclusions, and recommendations are those of the authors and do not necessarily reflect the views of the National Oceanic and Atmospheric Administration (NOAA), U.S. Department of Commerce.

9. REFERENCES

Black, T. L., D. G. Deaven, and G. J. DiMego, 1993: The step-mountain eta-coordinate model: 80-km "early" version and objective verifications. NWS Technical Procedures Bulletin 412, NOAA/NWS, 31 pp. [Available from National Weather Service, Office of Meteorology, 1325 East-West Highway, Silver Spring, MD 20910]

Gill, A. E., 1982: *Atmosphere-Ocean Dynamics*. Academic Press, 662 pp

Janjic, Z. L., 2004: [The NCEP WRF core](#). Preprints, 20th Conference on Weather Analysis and Forecasting/16th Conference on Numerical Weather

Prediction, Seattle, WA, Amer. Meteor. Soc., on CD-ROM

Janjic, Z. L., J. P. Gerrity Jr., and S. Nickovic, 2001: An alternative approach to nonhydrostatic modelling. *Mon. Wea. Rev.*, **129**, 1164-1178

NCEP, cited 2007: [Log of operational model changes](#). Available online at <http://www.emc.ncep.noaa.gov/mmb/research/eta.log.html>

NCEP, cited 2007b: Online documentation of major changes. Available online at <http://www.emc.ncep.noaa.gov/mmb/mmbpll/eric.html#TAB4>

Rogers, E, M. Ek, B. Ferrier, G. Gayno, Y. Lin, K. Mitchell, M. Pondeca, M. Pyle, C. Wong, and W. Wu, 2005: [The NCEP North American Mesoscale Modeling System: Final Eta model/analysis changes and preliminary experiments using the WRF-NMM](#). *Extended Abstracts, AMS 17th Conf. on Numerical Weather Prediction, Wash. D.C.*

WRF, cited 2007: The Weather Research and Forecasting Model. Available online at <http://www.wrf-model.org/>